Monthly Notices of the ROYAL ASTRONOMICAL SOCIETY

MNRAS **503,** 5448–5454 (2021) doi:10.1093/mnras/stab799
Advance Access publication 2021 March 19

3C 84: a possibly precessing jet in 43-GHz observations

Rune M. Dominik ,★ Lena Linhoff , Dominik Elsässer and Wolfgang Rhode
Department of Physics, TU Dortmund University, D-44227 Dortmund, Germany

Accepted 2021 March 12. Received 2021 March 12; in original form 2020 December 22

ABSTRACT

The central galaxy of the Perseus galaxy cluster, 3C 84 or NGC 1275, hosts one of the closest and well-observed active galactic nuclei (AGNs) and thus offered insights into a variety of phenomena over the past decades. Although close and well observed, some key properties of 3C 84 remain unknown. One of these properties is the inclination angle between the jet and the line of sight, for which a wide range of values can be found in publications. Previous studies have indicated a precessing behaviour of 3C 84's jet that could explain these discrepancies. In this work, we analyse this behaviour at parsec scales using VLBA-BU-BLAZAR Program 43-GHz data. To obtain the position angles necessary to deduce the precessing motion, we use a primary component analysis to extract angles from the available images. The model parameters are estimated through Bayesian Inference. A clear change in the position angle is visible in our data, consistent with a precession. For a pure, non-relativistic precession model, we find a precession frequency of $(12.5 \pm 1.8)^\circ\,\mathrm{yr}^{-1}$. We further test the possibility of an additional nutation but can, so far, not obtain conclusive results.

Key words: galaxies: individual: 3C 84 – galaxies: jets – galaxies: kinematics and dynamics.

1 INTRODUCTION

The radio counterpart 3C 84 ($z = 0.0176$) of the central galaxy of the Perseus cluster, NGC 1275, has been subject to numerous observations. Classified as Fanaroff–Riley type-I, this active galactic nucleus (AGN) features an almost cylindrical, limb-brightened jet in 43-GHz observations, that has presumably formed in a restarting event in 2005 (Nagai et al. 2014). 3C 84's radio core at 43 GHz reveals three main constituents: The radio core C1 and two jet components C2 and C3 (Suzuki et al. 2012).

Despite all efforts, inconsistent values for its inclination angle, the angle between the jet axis and the line of sight, were reported in previous publications. Very Long Baseline Interferometry (VLBI) experiments calculated this angle to be 30–55° (Walker, Romney & Benson 1994), 11° (Lister et al. 2009), and $(64 \pm 16)^\circ$ (Fujita & Nagai 2016). Krichbaum et al. (1992) found a strongly bent jet, whose inclination angle changes from $\leq 2.7^\circ$ on a milli-arcsecond scale up to 39.4–58.2° on an arcsecond scale. In the gamma-ray regime, *Fermi*-LAT reported an inclination of 25° (Abdo et al. 2009) while MAGIC found an angle $\leq 12^\circ$ (Ansoldi et al. 2018). These seemingly disagreeing values could be consistent if 3C 84's jet is precessing, something that has been indicated in X-ray observations by Dunn, Fabian & Sanders (2006) and Falceta-Gonçalves et al. (2010) and, most recent, in radio light curves by Britzen et al. (2019).

To probe the possibility of a precessing jet, Section 2 will summarize the geometric relations between the inclination angle and the jet's position angle. In Section 3, we will propose an automated algorithm using a primary component analysis to extract the position angles from the Boston University Blazar Monitoring Program (VLBA BU-BLAZAR) observations (Jorstad & Marscher 2016) and use the model described in the previous Section to estimate the model parameters. Section 4 will discuss the possibility of an additional nutation overlaying the precession and Section 5 will summarize and conclude our findings.

2 JET PRECESSION MODELLING

While the true precessing motion of an AGN's jet will lie intrinsically in three dimensions, astronomical observations can only present a 2D projection of this process. A direct observation of a changing inclination angle ϕ is, therefore, not possible. Accessible through observations are changes in the projected AGN's jet's position angle η, the angle between the jet and an arbitrary reference line in the image plane, as seen in Fig. 1. To connect both quantities, Caproni & Abraham (2004) expressed ϕ and η in a Cartesian coordinate frame:

$$\phi(t) = \arcsin \sqrt{x(t)^2 + y(t)^2} \tag{1}$$

$$\eta(t) = \arctan \tfrac{y(t)}{x(t)}. \tag{2}$$

Expressions for x and y can be obtained through a set of rotations, transforming the movement from a Cartesian coordinate frame (hereafter indicate by the *tilde*), where the $\tilde{z}$-axis is given through the precession axis (η_0, ϕ_0), back to a frame, where the z-axis is given through the line of sight on to the source. As for the measurement of position angles, the following equations will express them relative to the y-axis in Fig. 1 to achieve conformity with Caproni & Abraham (2004). It is shown in Appendix A that our measurement clockwise and relative to the north–south axis (x in Fig. 1) results in an invariant set of equations.

★ E-mail: rune.dominik@tu-dortmund.de

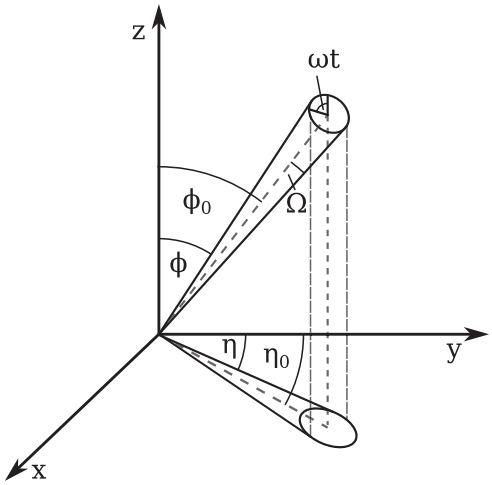

Figure 1. Precession model in three dimensions as seen in Carrara et al. (1993) using their reference system. The observer looks along the z-axis on to the 3D motion. For every moment, the jet moves on the circle shown, forming the precession cone, whose axis is displayed as dashed line. Observations are made in the xy-plane.

On a unit sphere in the *tilded* frame, the jet precesses on a circle with radius

$$\tilde{\boldsymbol{r}} = \begin{pmatrix} \tilde{x} \\ \tilde{y} \\ \tilde{z} \end{pmatrix} = \begin{pmatrix} \sin\Omega \sin\omega(t-t_0) \\ \sin\Omega \cos\omega(t-t_0) \\ \cos\Omega \end{pmatrix}. \tag{3}$$

This motion can then be expressed in the *un-tilded* frame using the two rotations $\mathbf{R}_z$ and $\mathbf{R}_y$:

$$\boldsymbol{r} = \begin{pmatrix} x \\ y \\ z \end{pmatrix} = \mathbf{R}_z(\eta_0)\mathbf{R}_y(\phi_0)\tilde{\boldsymbol{r}} \tag{4}$$

$$= \begin{pmatrix} \cos\eta_0 & -\sin\eta_0 & 0 \\ \sin\eta_0 & \cos\eta_0 & 0 \\ 0 & 0 & 1 \end{pmatrix} \begin{pmatrix} \cos\phi_0 & 0 & \sin\phi_0 \\ 0 & 1 & 0 \\ -\sin\phi_0 & 0 & \cos\phi_0 \end{pmatrix} \tilde{\boldsymbol{r}} \tag{5}$$

$$= \begin{pmatrix} A(t)\cos\eta_0 - B(t)\sin\eta_0 \\ A(t)\sin\eta_0 + B(t)\cos\eta_0 \\ -\sin\phi_0 \sin\Omega \sin\omega(t-t_0) + \cos\phi_0 \cos\Omega \end{pmatrix} \tag{6}$$

with

$$A(t) = \cos\Omega \sin\phi_0 + \sin\Omega \cos\phi_0 \sin\omega(t-t_0) \text{ and} \tag{7}$$

$$B(t) = \sin\Omega \cos\omega(t-t_0). \tag{8}$$

In this set of equations, the precession cone half opening angle Ω, the precession frequency ω, the precession axis inclination angle ϕ_0, the precession axis position angle η_0 and the reference phase t_0 act as model parameters. Since the inclination and position angle are not directly dependent on each other, equation (2) can be used to estimate these parameters to then constrain the inclination ϕ through equation (1).

It is imperative to mention that this set of equations is intrinsically defined in the reference frame fixed at the source (denoted, hereafter, by the *prime*) while any measurement is taken in the observer's frame (see i.e. Abraham 2000). Assuming a relativistic jet, the transition between these two reference frames for a time t is given by Zhang & Li (2018)

$$\mathrm{d}t' = \delta \mathrm{d}t \tag{9}$$

with the Doppler factor δ. A constant δ results in the often used $t' = \delta t$ equation, a time-dependent Doppler factor, however, requires for solving this integration. Since the Doppler factor is given by

$$\delta = (\gamma(1 - \beta\cos\phi'))^{-1} = \gamma(1 + \beta\cos\phi) \tag{10}$$

with the Lorentz factor γ and the inclination ϕ is time dependent due to equation (1), integration is necessary in the precessing case. As we will only obtain measurements for η in the observer's frame (see Section 3), we have no direct handle on the ϕ regime and are, therefore, unable to solve this integration in a meaningful way without producing an overly complicated model. As a consequence, we will assume a non-relativistic jet for 3C 84 whenever we derive quantitative results hereafter. This assumption is in agreement with reported jet component speeds of $\beta \approx 0.23\,c$ found by Fujita & Nagai (2016) or 0.3 c–0.5 c in Walker et al. (2000) and we expect only minor deviations if these speeds hold true for the jet in general. However, considerably higher speeds outside jet features like the C3 component are possible. Naturally, any quantitative result from a non-relativistic model can only be treated as approximation in the case of a relativistic jet, whereas qualitative results remain unchanged.

3 DATA EXTRACTION AND PARAMETER ESTIMATION

Fig. 2 shows three epochs taken from more than 9 yr of VLBA-BU-BLAZAR Program observations available for 3C 84. The position angle is changing from a positive (measured clockwise relative to a vertical axis) to a negative value over the displayed period. To extract the needed position angle from the 3C 84 observations provided by the VLBA-BU-BLAZAR Program in a reproducible manner, we invented an automated approach without user interaction.

3.1 Extraction procedure

In a first pre-processing step, we use DIFMAP (Shepherd 1997) to re-image all observations to a common resolution of (0.01×0.01) marcsec^2 on a (1024×1024) px grid. Furthermore, we restore all images to a common, circular beam with a diameter of 0.28 marcsec, the major axis of the beam present in all but three of the used epochs. This restoring is done to prevent biasing the extracted position angles through the original beam's orientation angle. We then use SCIKIT-IMAGE's (van der Walt et al. 2014) blob detection and random walker segmentation algorithm on all pixels with a flux higher than 2.5 per cent of the brightest pixel in order to find 3C 84's C1 component and select the innermost parts of the jet. We have chosen the value of 2.5 per cent as we are only interested in the brightest parts of the images, namely the central component and the jet base. The chosen value is above the noise level for all but one epoch (the epoch 2012 January 27 was, therefore, excluded from further analysis). Hence, using this threshold reliably cuts off noise and suppresses structures of low intensity that would otherwise obscure the segmentation. With this suppression, the segmentation can be used on noisy images, as long as the noise level is below this threshold.

Using the segmented area, we apply a primary component analysis in order to parametrize it as a 2D Gaussian. With its major and minor axis, the Gaussian's position angle can be computed relatively to a vertical reference axis. We treat this angle as jet position angle. A similar identification of the position angle was performed with fitted Gaussians by Martí-Vidal et al. (2011) to investigate a precessing jet in M 81.

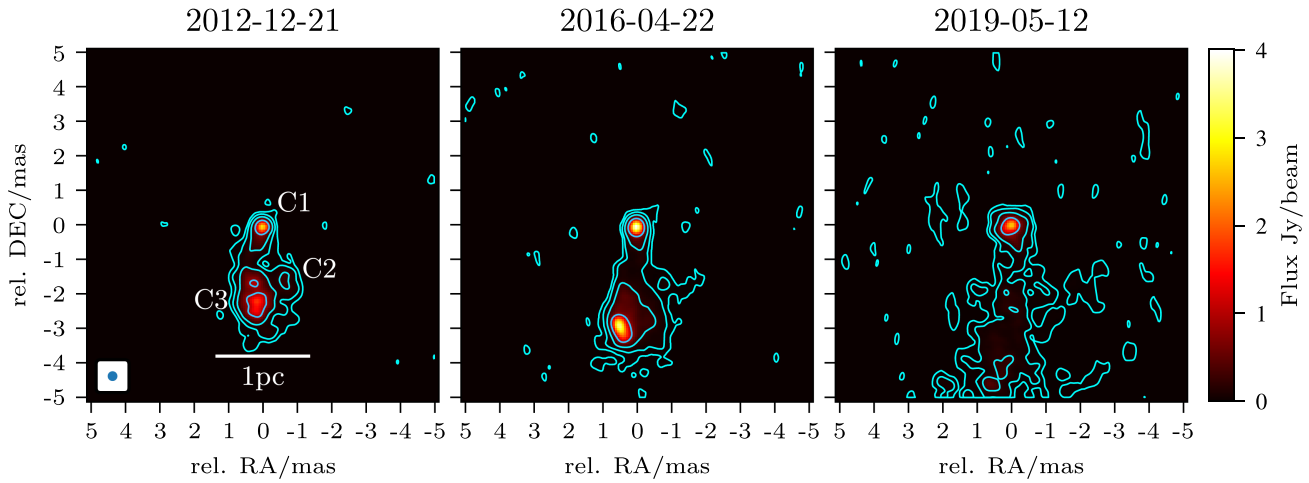

Figure 2. Three epochs of 3C 84 observations from the VLBA-BU-BLAZAR program with a visible change in the AGN's jet position angle. Colourbar, logarithmic contours, and circular beam are fixed for all images, contour levels at (0.01, 0.04, 0.02, 0.89, and 4.01) Jy beam^{-1} (rounded). Scale under the assumption of $H_0 = 69\,\mathrm{km\,Mpc^{-1}\,s^{-1}}$.

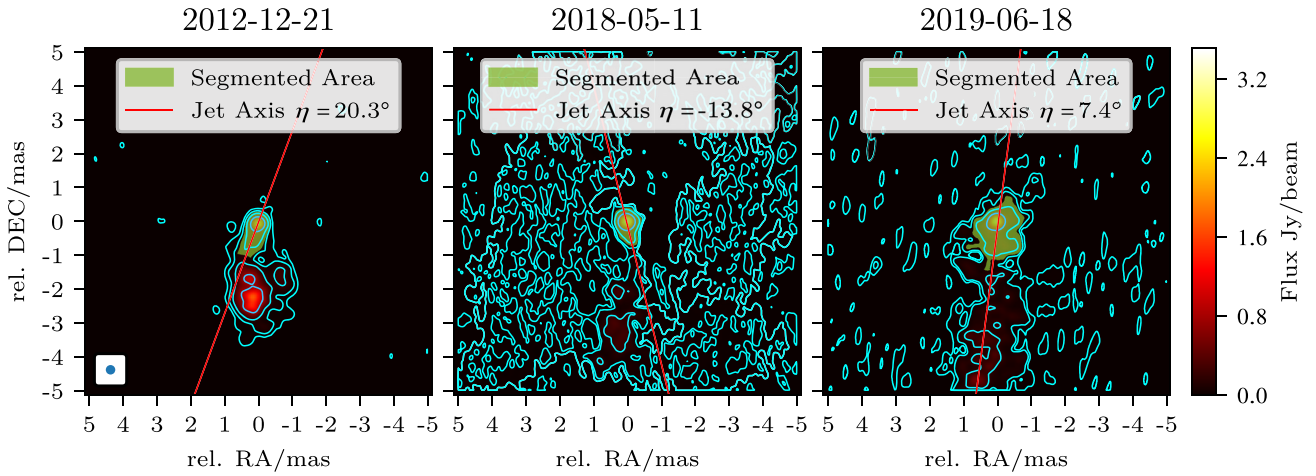

Figure 3. Three epochs of 3C 84 observations from the VLBA-BU-BLAZAR program with overlayed segmented area and estimated jet axis. Colourbar, logarithmic contours, and circular beam are fixed for all images, contour levels at (0.01, 0.04, 0.02, 0.80, and 3.51) Jy beam^{-1} (rounded). *Left:* Good quality epoch. *Mid:* Noisy epoch. *Right*: Epoch with indistinct jet base.

To illustrate this process and highlight its limits, Fig. 3 shows three epochs of 3C 84 observations with their corresponding segmented area and reconstructed jet axis. While a jet axis can be reconstructed for an image of good quality as well as for noisy images, the epoch shown in the right-hand panel of Fig. 3 does not allow for a clear identification of the jet base as the central stucture appears washed out to a roundish shape.

3.2 Model fitting

To estimate the precession-model parameters, we use a two stage Bayesian inference approach in PYMC3 (Salvatier, Wiecko & Fonnesbeck 2016). This method utilizes a Markov chain Monte Carlo (MCMC) sampler to explore the parameter space efficiently and then compute an a posteriori probability for each accepted point through Bayes' theorem. As present in Bayes' theorem, a likelihood that encodes the agreement between a model and the actual data has to be constructed and priors have to be defined. After usage, the mode of the posterior distribution, the maximum a posteriori value, can be used as estimation for the model parameters. Additionally, information about these parameters' uncertainties can be derived from the posterior. A huge advantage of this method is its applicability even to complex models, where traditional fitting methods fail. A more in-depth insight can be found e.g. in Veitch et al. (2015).

In a first step, we simultaneously fit the precession parameters in a Cartesian frame. Transforming η, which is measured relative to the x-axis in Fig. 1, from a polar frame back into a Cartesian frame, two Gaussian distributions $\mathcal{N}$ can be used as prior assumptions for the distribution of the obtained data points:

$$\cos\eta_{\mathrm{obs}}(t) \sim \mathcal{N}(\mu_x, \sigma_x^2) \tag{11}$$

$$\sin\eta_{\mathrm{obs}}(t) \sim \mathcal{N}(\mu_y, \sigma_y^2), \tag{12}$$

where μ_x and μ_y are given through

$$\mu_x = \frac{x(t)}{\sqrt{x(t)^2+y(t)^2}} \tag{13}$$

Table 1. Uniform prior boundaries for both models.

Parameter	Lower limit	Upper limit	Unit
Ω	0	45	$^\circ$
ω	0	20	$^\circ\,\mathrm{yr}^{-1}$
t_0	−30	10	yr
ϕ_0	0	180	$^\circ$
η_0	−90	90	$^\circ$
σ_x, σ_y, and σ_η	0	20	$^\circ$
A_{nut}	0	15	$^\circ$
ω_{nut}	80	260	$^\circ\,\mathrm{yr}^{-1}$
$t_{0,\,\mathrm{nut}}$	−3	3	yr

Table 2. Derived precession parameters for both models.

Parameter	Without nutation	With nutation	Units
Ω	22.7 ± 4.0	19.3 ± 1.7	$^\circ$
ω	12.5 ± 1.8	16.8 ± 1.1	$^\circ\,\mathrm{yr}^{-1}$
t_0	− 1.2 ± 1.2	− 6.0 ± 0.7	yr
ϕ_0	54.4 ± 15.2	81.2 ± 12.0	$^\circ$
η_0	− 0.6 ± 4.3	2.3 ± 1.4	$^\circ$
σ	4.0 ± 0.4	3.4 ± 0.3	$^\circ$
A_{nut}	–	2.9 ± 0.7	$^\circ$
ω_{nut}	–	106.3 ± 5.4	$^\circ\,\mathrm{yr}^{-1}$
$t_{0,\,\mathrm{nut}}$	–	− 1.8 ± 0.4	yr

$$\mu_y = \frac{y(t)}{\sqrt{x(t)^2+y(t)^2}} \tag{14}$$

using x and y from equation (4). Such a choice is necessary to construct the likelihood. We assume η_{obs} to be sampled form a normal distribution centered at an unknown truth with an unknown deviation. The deviations σ_x and σ_y can be interpreted as nuisance parameters and allow for an estimation of a systematic measurement error. With uniform priors on the parameters, whose boundaries are displayed in Table 1, we sample 10 000 (+10 000 burn-in) points on 12 MCMC chains each using a No-U-Turn sampler, a self tuning extension to Hamilton Monte Carlo (Hoffman & Gelman 2014). We then use the mode and half the standard deviation of each parameter's posterior landscape as mean and deviation for truncated Gaussian priors, replacing the uniform priors for all physical parameters in a second fitting step. This second fitting step is done directly in the η regime, swapping the priors (11) and (12) to a common prior

$$\eta_{\mathrm{obs}} \sim \mathcal{N}\left(\eta(t), \sigma_\eta^2\right), \tag{15}$$

where $\eta(t)$ is given through equation (2). In this step, 12 chains sample 5000 (+5000 burn-in) points each using a No-U-Turn sampler. Our estimation result is then given by the sample modes and an uncertainty estimation is given through the sample deviations. While a single step approach with uniform priors should suffice if one has a sufficient amount of data points, we resort to our two-step solution to justify the choice of the Gaussian parameter priors that are needed to account for the limited statistic available.

3.3 Results

Using the algorithm described above on all but four[1] of the available VLBA-BU-BLAZAR epochs between 2010 November 1 and 2020 January 3, we derive a precession with a frequency of $(12.5 \pm 1.8)^\circ\,\mathrm{yr}^{-1}$ which corresponds to a period of ≈ 28.8 yr and a precession cone half opening angle of $(22.7 \pm 4.0)^\circ$. An overview over all fitted parameters can be found in Table 2. The extracted position angles are displayed alongside the fitted model in Fig. 4. The re-imaged BU-BLAZAR observations are provided in Appendix B with the estimated jet position angles. All autocorrelations decrease and approach zero on scales of $\mathcal{O}(10)$ so we find our choice of burn-in samples has been made in excess. As the $\hat{R}$-statistic (Brooks & Gelman 1998) reads 1 reliably for all non-periodic parameters, we find no signs for a failed convergence of the fitting process. They show a clear decrease without any visible outliers, a strong sign for

[1]Two of the unused epochs (2019 June 19 and 2019 July 1) show insufficient image quality. The epoch 2012 January 27 was excluded due to a high noise level. The epoch 2015 August 01 missed a necessary file.

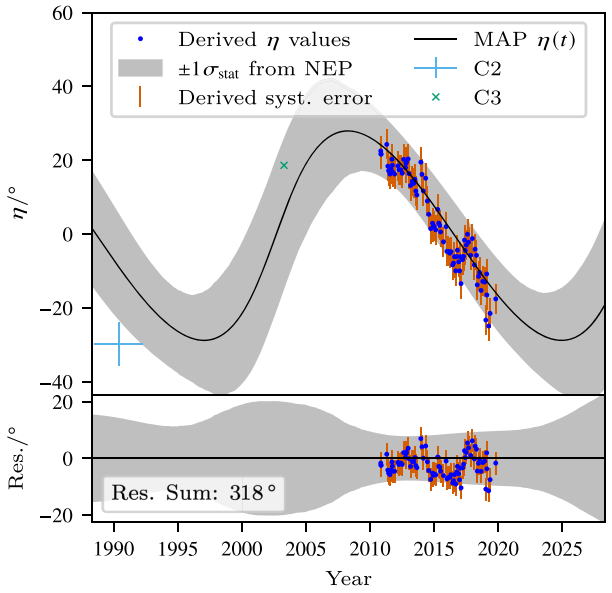

Figure 4. Extracted position angles with fitted model. The statistical error σ_{stat} is obtained through numerical error propagation (NEP).

the viability of the extraction algorithm. In addition to the steady decrease in the position angle, another periodicity seems overlaying the pure precession with peaks around 2013, 2016, and 2018. This can be interpreted as a sign for a nutational motion.

To apply a minimal cross check of our results, we use the information provided by Suzuki et al. (2012) for the C2 and C3 jet components. Both data points are in agreement with our estimation with respect to their uncertainty. Our estimation is therefore able to explain the ejection angle of both epochs. More detailed information on these two data points is given in Appendix C.

Using the found model parameters to compute the inclination angle for 3C 84 results in the curve plotted in Fig. 5 alongside the previously published ϕ values mentioned in Section 1. While our estimation does not match all of these results, it yields inclinations that are within a reasonable range.

4 NUTATION

As mentioned before, an additional periodicity overlaying the position angle decrease is visible in our data. To include such a motion into the precession model, we follow the same idea used to derive the former model. As discussed by Britzen et al. (2018), we start with a motion in a frame using the nutation axis as $\tilde{z}$-axis and then

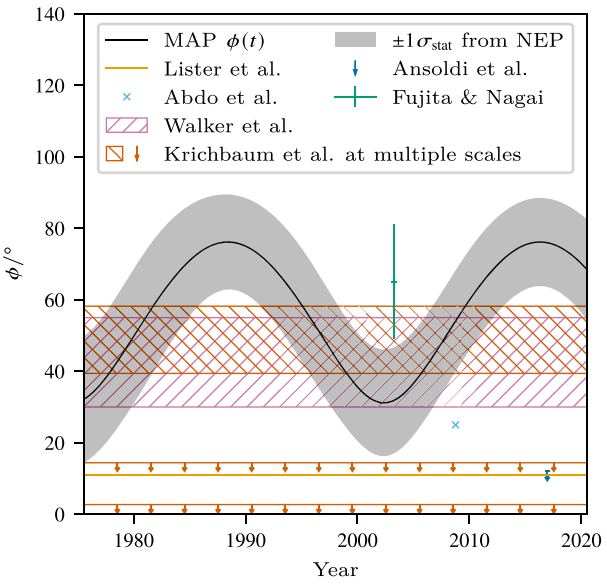

Figure 5. Computed inclination angles from the fitted model.

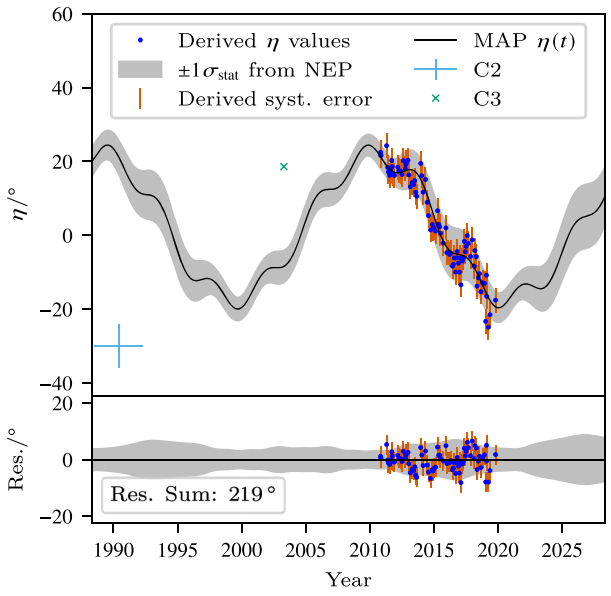

Figure 6. Extracted position angles with fitted nutation model.

apply four rotations to transform the motion back into the precessing frame at first and then into the desired frame fixed through the line of sight. With the nutation cone half opening angle $A_{\rm nut}$, the nutation frequency $\omega_{\rm nut}$, and a nutation reference phase $t_{0,\,\rm nut}$, the position vector in the *tilded* frame is given as

$$\tilde{\boldsymbol{r}} = \begin{pmatrix} \tilde{x} \\ \tilde{y} \\ \tilde{z} \end{pmatrix} = \begin{pmatrix} \sin A \sin \omega_{\rm nut} \left(t - t_{0,\,\rm nut}\right) \\ \sin A \cos \omega_{\rm nut} \left(t - t_{0,\,\rm nut}\right) \\ \cos A \end{pmatrix} \tag{16}$$

and is linked to the *un-tilded* frame via

$$\boldsymbol{r} = \mathbf{R}_z(\eta_0)\mathbf{R}_y(\phi_0)\mathbf{R}_z\left(\omega(t - t_0)\right)\mathbf{R}_y(\Omega)\tilde{\boldsymbol{r}}. \tag{17}$$

Again, we will assume a non-relativistic jet when using this model.

We use the results (mode and deviation) of the precession results as prior for the precession parameters and additional uniform priors amplitude, nutation frequency, and nutation reference phase as given in Table 1 in a 12 chain MCMC setting with 5000 (+5000 burn-in) samples per chain. Some remarks are in order regarding this prior choice. First, the prior boundaries for the nutation frequency excludes long (period over 4.5 yr) and small-scale (period under 1.4 yr) motions. This upper limit was chosen to represent the limited time-span, where data from the VLBA-BU-BLAZAR Program is available while the lower limit is intended to account for the limited amount of data points per year. Secondly, and more importantly, the usage of the precession estimations results in an improved convergence but leaves both results dependent on each other. Our nutation results should therefore be seen as an extension of the pure precession and not as an alternative model.

Using this model, we find a precessing frequency of $(16.8 \pm 1.1)^\circ\,\mathrm{yr}^{-1}$ (period of ≈21.4 yr), a half opening angle of $(19.3 \pm 1.7)^\circ$, a precession cone half opening angle of $(2.9 \pm 0.7)^\circ$, and a nutation frequency of $(106.3 \pm 5.4)^\circ\,\mathrm{yr}^{-1}$ (period of ≈3.4 yr). All other fitted parameters can again be found in Table 2. Again, autocorrelations that quickly approach zero and $\hat{R}$-statistics reading one indicate convergence and a sufficiently long burn-in phase. However, we needed to exclude several chains as they have converged to alternative values for the periodic quantity $t_{0,\rm nut}$, as $t_{0,\rm nut}$ can only be estimated modulo the nutation period. The estimations for all other parameters do, however, agree in their respective error estimations over all chains.

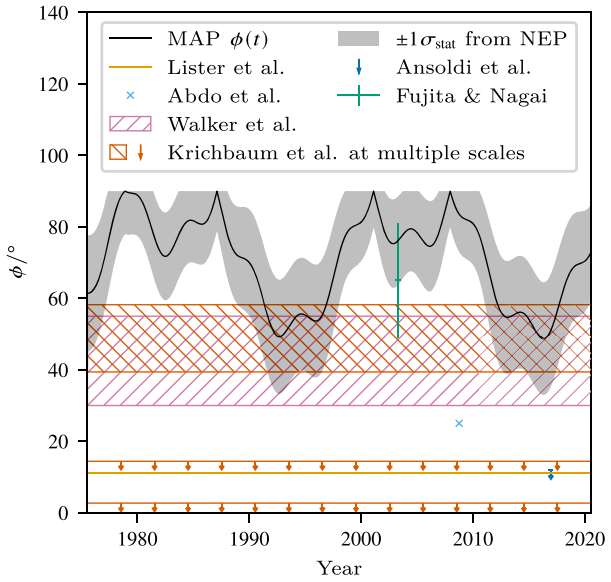

Figure 7. Computed inclination angles from the fitted model with nutation. The folding of inclinations over 90° back to inclinations below 90° is due to the restriction of the sine-function to values in [−90° , 90°] to be invertible.

While the new model follows the extracted position angles more closely, as visible in Fig. 6 and compared to Fig. 4, it cannot explain the position angles of the C2 and C3 component. Furthermore, the computed inclination angles are considerably higher than most published values in Fig. 7 and even exceed 90° – a behaviour not indicated through the imaged epochs where nowhere no counterjet is visible. Most probably, the limited amount of data do not yield meaningful results in a more complex model and a classical overfitting problem arises. The possibility of an additional nutation should be revisited

when more data are available. As of now, no evidence for a nutation can be found.

5 CONCLUSIONS

In this paper, we have proposed a method to extract jet position angles from VLBI radio observations and used the obtained data to estimate precession parameters for 3C 84 using two non-relativistic models, one with a pure precession and another with an additional nutation.

5.1 Position angle estimation

Our proposed method to extract position angles via primary component analysis yields good results for 3C 84. This AGN is, on the other hand, a somewhat unique source. With its extended appearance and clearly visible, cylindrical jet, the position angle estimation is not too difficult, but a segmentation of the beginning jet is necessary. This step should be redundant if this approach is used on compact sources like OJ 287, another AGN with previously discussed precession (Britzen et al. 2018). Compared with more traditional methods, namely the identification of components inside the jet and tracing them back to their angle and time of ejection, our method results in one measurement per observation instead of per component. Furthermore, our method does not require user interaction and is automatable, while the fitting of components inside the jet is typically done by hand.

5.2 Precession in the AGN 3C 84

Since a clear change of the position angle is visible both by quantitative comparison of different observation epochs and qualitative in the extracted data, a precessing jet is among the possible explanations for this behaviour. We find that a precession on time-scales between 25 and 30 yr can describe the observed change, although the available amount of data does not include one full precession period. This time-scale is, compared to existing publications, extremely short. While Britzen et al. (2019) report precession periods up to 101 yr from radio light curves, Dunn et al. (2006) and Falceta-Gonçalves et al. (2010) find periods on the scale of Myr from X-ray data. The seemingly contradicting results of the latter mentioned publications and this work could either be an indication for a strongly accelerated precession or both results show two different processes. As for the signs for an additional nutation, we conclude that such a motion is very well possible due to the complex gravitational landscape in an AGN's vicinity. At this point, we are not able to provide reliable estimations for a nutation. We again want to stress that quantitative results were obtained through non-relativistic models. The qualitative result that the change in 3C 84's jet positioning angle is visible from the observations, indicating a precessing jet remains unaffected.

We find our work's results to be a strong indication for a precessing jet, although we cannot rule out scenarios like jet reorientation as discussed by Babul, Sharma & Reynolds (2013). If the evidence for a precessing jet would tighten, this would be a strong sign for a binary black hole system inside 3C 84's centre.

ACKNOWLEDGEMENTS

We thank Alexander Sandrock for fruitful discussions and comments. We further thank an anonymous referee for important and constructive comments.

This study makes use of 43 GHz VLBA data from the VLBA-BU Blazar Monitoring Program (VLBA-BU-BLAZAR; http://www.bu.edu/blazars/VLBAproject.html), funded by NASA through the Fermi Guest Investigator Program. The VLBA is an instrument of the National Radio Astronomy Observatory. The National Radio Astronomy Observatory is a facility of the National Science Foundation operated by Associated Universities, Inc.

Part of the work on this paper has been supported by Deutsche Forschungsgemeinschaft (DFG) – project number 124020371 – within the Collaborative Research Center **(Sonderforschungsbereich)** SFB 876 'Providing Information by Resource-Constrained Analysis', DFG project number 124020371, SFB project C3.

DATA AVAILABILITY

The data used in the main part of this work was taken from the VLBA-BU-BLAZAR Program and can be accessed and downloaded from https://www.bu.edu/blazars/VLBA_GLAST/0316.html. The data used for the additional cross check have been published by Suzuki et al. (2012).

REFERENCES

Abdo A. A. et al., 2009, ApJ, 699, 31
Abraham Z., 2000, A&A, 355, 915
Ansoldi S. et al., 2018, A&A, 617, A91
Babul A., Sharma P., Reynolds C. S., 2013, ApJ, 768, 11
Britzen S. et al., 2018, MNRAS, 478, 3199
Britzen S., Fendt C., Zajacek M., Jaron F., Pashchenko I., Aller M. F., Aller H. D., 2019, Galaxies, 7,72
Brooks S. P., Gelman A., 1998, J. Comput. Graph. Stat, 7, 434
Caproni A., Abraham Z., 2004, MNRAS, 349, 1218
Carrara E. A., Abraham Z., Unwin S. C., Zensus J. A., 1993, A&A, 279, 83
Dunn R. J. H., Fabian A. C., Sanders J. S., 2006, MNRAS, 366, 758
Falceta-Gonçalves D., Caproni A., Abraham Z., Teixeira D. M., de Gouveia Dal Pino E. M., 2010, ApJ, 713, L74
Fujita Y., Nagai H., 2016, MNRAS, 465, L94
Hoffman M. D., Gelman A., 2014, J. Mach. Learn. Res., 15, 1593
Jorstad S., Marscher A., 2016, Galaxies, 4, 47
Krichbaum T. P. et al., 1992, A&A, 260, 33
Lister M. L. et al., 2009, AJ, 138, 1874
Martí-Vidal I., Marcaide J. M., Alberdi A., Pérez-Torres M. A., Ros E., Guirado J. C., 2011, A&A, 533, A111
Nagai H. et al., 2014, ApJ, 785, 53
Salvatier J., Wiecko T. V., Fonnesbeck C., 2016, PeerJ Comput. Sci., 2, e55
Shepherd M. C., 1997, in Hunt G., Payne H., eds, ASP Conf. Ser., Vol. 125, Astronomical Data Analysis Software and Systems VI. Astron. Soc. Pac., San Francisco, p. 77
Suzuki K. et al., 2012, ApJ, 746, 140
van der Walt S., Schönberger J. L., Nunez-Iglesias J., Boulogne F., Warner J. D., Yager N., Gouillart E., Yu T., 2014, PeerJ, 2, e453
Veitch J. et al., 2015, Phys. Rev. D, 91, 042003
Walker R. C., Romney J. D., Benson J. M., 1994, ApJ, 430, L45
Walker R. C., Dhawan V., Romney J. D., Kellermann K. I., Vermeulen R. C., 2000, ApJ, 530, 233
Zhang B., Li K., 2018, ApJ, 854, 123

SUPPORTING INFORMATION

Supplementary data are available at *MNRAS* online.

Appendix B. Re-imaged 3C 84 Observations.

Please note: Oxford University Press is not responsible for the content or functionality of any supporting materials supplied by the authors.

Any queries (other than missing material) should be directed to the corresponding author for the article.

APPENDIX A: INVARIANCE OF THE REFERENCE SYSTEMS

Changing the reference system used by Caproni & Abraham (2004) towards our reference system can be done by using

$$\eta = \tfrac{\pi}{2} + \eta' \text{ and} \tag{A1}$$

$$\eta_0 = \tfrac{\pi}{2} + \eta_0', \tag{A2}$$

where the *prime* denotes our measurement. Finding that

$$\cos\eta_0 = \cos\tfrac{\pi}{2} + \eta_0' = -\sin\eta_0', \tag{A3}$$

$$\sin\eta_0 = \sin\tfrac{\pi}{2} + \eta_0' = \cos\eta_0', \text{ and} \tag{A4}$$

$$\tan\eta = \tan\tfrac{\pi}{2} + \eta' = -\cot\eta' \tag{A5}$$

we can transform x and y so that

$$x' = x\left(\eta_0 = \frac{\pi}{2} + \eta_0'\right) = -A\sin\eta_0' - B\cos\eta_0' = -y(\eta_0 \to \eta_0') \tag{A6}$$

and

$$y' = y\left(\eta_0 = \frac{\pi}{2} + \eta_0'\right) = A\cos\eta_0' - B\sin\eta_0' = x(\eta_0 \to \eta_0'). \tag{A7}$$

With equations (A5)–(A7), we can fully transform the used equations to our reference system

$$\tan\eta = \frac{y}{x} \to -\cot\eta' = \tfrac{y'}{x'} = -\tfrac{x(\eta_0\to\eta_0')}{y(\eta_0\to\eta_0')} \tag{A8}$$

$$\Rightarrow \tan\eta' = \tfrac{y(\eta_0\to\eta_0')}{x(\eta_0\to\eta_0')} \tag{A9}$$

and, therefore, find the model to be invariant if η is replaced with our η'.

APPENDIX B: RE-IMAGED 3C 84 OBSERVATIONS

Appendix B contains images of all available epochs, re-imaged to a circular beam with estimated jet position angle. This Appendix is provided online.

APPENDIX C: EJECTION ANGLE AND EPOCH FOR THE C2 AND C3 COMPONENT

To provide a minimal cross check for our position angle estimation we use the ejection angle and epoch of 3C 84's two prominent jet components C2 and C3 (see Fig. 2 for reference) as the jet component's position angle should not change imensly after ejection and reflect the jet's position angle at that time. As Suzuki et al. (2012) found, C3 apeared first in observations taken on 2003 November 20 while no observation of C3 is reported for the previous observation taken on 2003 January 12. In consequence, we use this interval to constrain the ejection time and use the given ejection angle of 18.6° (in our reference system) as the jet's position angle at that time. To constrain C2, we use the data provided in table 5 of Suzuki et al. (2012) to extrapolate the component's movement back to its ejection assuming a linear motion. Shifting the paper's data in a way that the first observation is taken as reference time, we obtain a linear model with a slope of (0.081 ± 0.012) marcsec yr^{-1} and an intercept of (0.94 ± 0.06) marcsec, resulting in an estimated ejection in 1990.4 ± 1.9. Using mean and standard deviation of the position angles as estimation for the ejection angle, we find a value of $(-29.9 \pm 5.9)°$ in our reference system. Both the linear extrapolation and the position angle estimation are shown in Fig. C1.

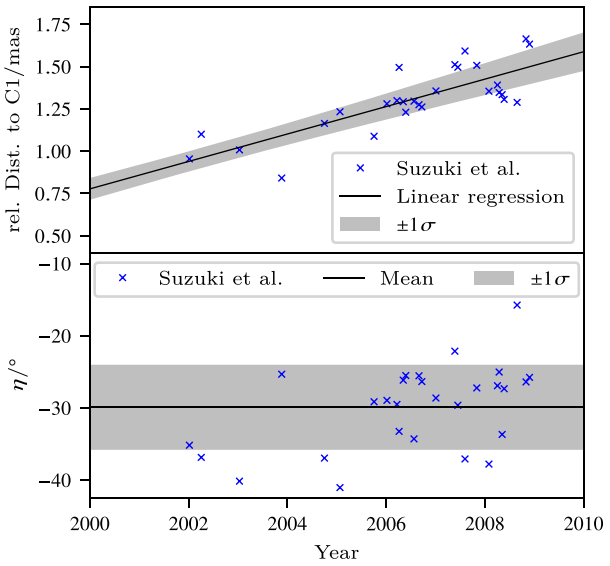

Figure C1. Data for 3C 84's C2 component computed from Suzuki et al. (2012). *Top:* Relative distance of the C2 component over time with linear regression. *Bottom:* Position angle of the C2 component with mean and standard deviation.

This paper has been typeset from a TEX/LATEX file prepared by the author.